Supplementary Information

Crinophagic granules in pancreatic β cells contribute to mouse autoimmune diabetes by diversifying pathogenic epitope repertoire

Hao Hu[1,#], Anthony N. Vomund[1,2,#], Orion J. Peterson[1,2], Neetu Srivastava[1,2], Tiandao Li[3], Lisa Kain[4], Wandy L Beatty[5], Bo Zhang[3], Chyi-Song Hsieh[6], Luc Teyton[4], Cheryl F. Lichti[1,2`], Emil R. Unanue[1,2,7], Xiaoxiao Wan[1,2,]*

[1]Department of Pathology and Immunology, Division of Immunobiology, Washington University School of Medicine, St. Louis, Missouri, USA.

[2]The Andrew M. and Jane M. Bursky Center for Human Immunology and Immunotherapy Programs, Washington University School of Medicine, St. Louis, Missouri, USA.

[3]Department of Developmental Biology, Center of Regenerative Medicine, Washington University School of Medicine, St. Louis, Missouri, USA.

[4]Department of Immunology and Microbiology, Scripps Research Institute, La Jolla, California, USA.

[5]Department of Molecular Microbiology, Washington University School of Medicine, St. Louis, Missouri, USA.

[6]Department of Internal Medicine, Division of Rheumatology, Washington University School of Medicine, St. Louis, Missouri, USA.

[7] Deceased.

[#]These authors contributed equally

**Corresponding author: wanx@wustl.edu.*

List of supplementary data

Supplementary figures S1-S9 and figure legends

Supplementary Data

- Supplementary Data 1 Peptide family for thymic MHC-II peptidome
- Supplementary Data 2 Individual peptide sequences identified in the thymic peptidome
- Supplementary Data 3 Tissue localization of the identified thymic MHC-II peptides
- Supplementary Data 4 PTAs corresponding to transcripts regulated by different factors
- Supplementary Data 5 Antibody information

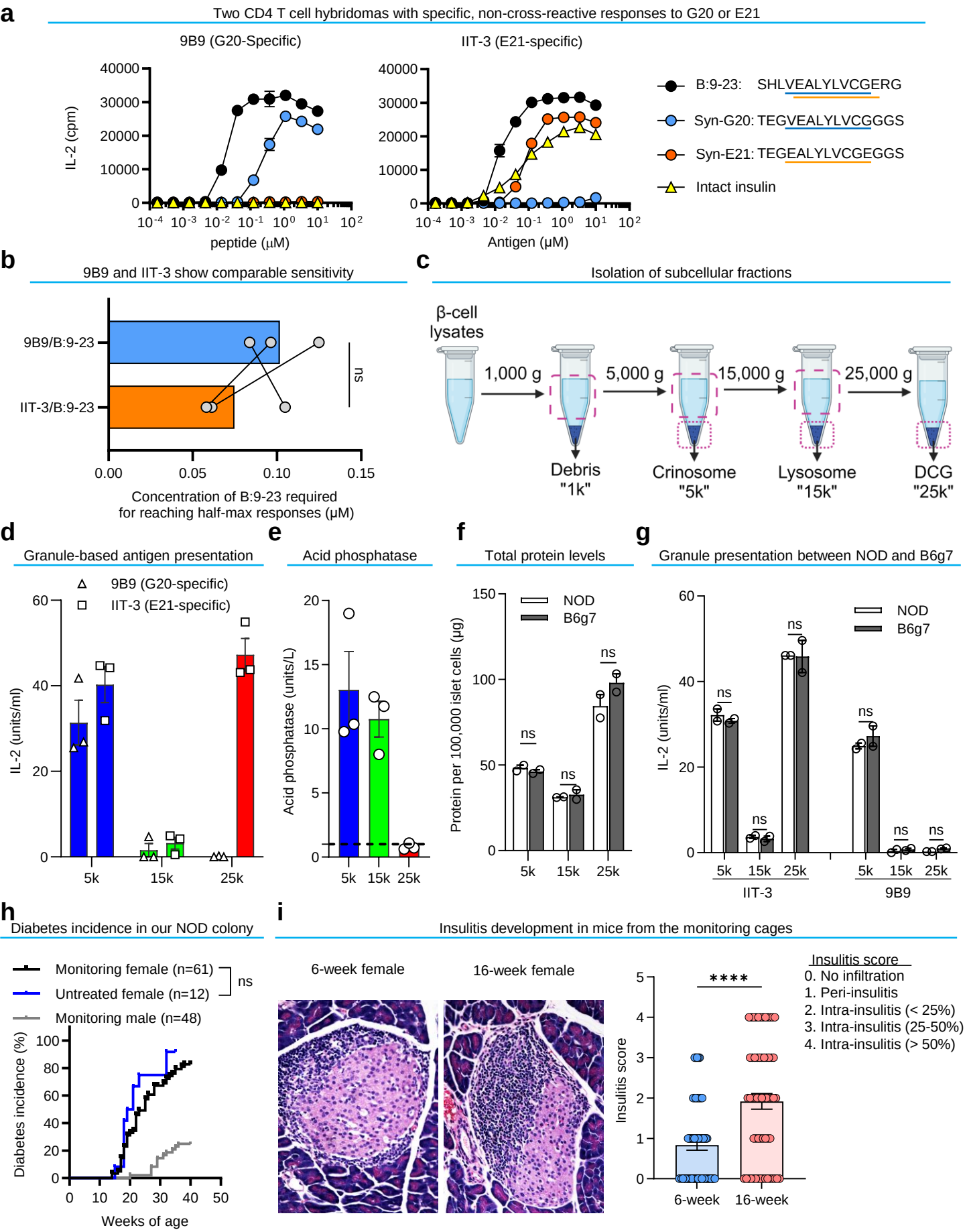
a
Two CD4 T cell hybridomas with specific, non-cross-reactive responses to G20 or E21
9B9 (G20-Specific)
IIT-3 (E21-specific)
IL-2 (cpm)
peptide (μM)
Antigen (μM)
B:9-23: SHLVEALYLVCGERG
Syn-G20: TEGVEALYLVCGGGS
Syn-E21: TEGEALYLVCGEGGS
Intact insulin
b
9B9 and IIT-3 show comparable sensitivity
9B9/B:9-23
IIT-3/B:9-23
ns
Concentration of B:9-23 required for reaching half-max responses (μM)
c
Isolation of subcellular fractions
β-cell lysates
1,000 g
5,000 g
15,000 g
25,000 g
Debris "1k"
Crinosome "5k"
Lysosome "15k"
DCG "25k"
d
Granule-based antigen presentation
9B9 (G20-specific)
IIT-3 (E21-specific)
IL-2 (units/ml)
e
Acid phosphatase
Acid phosphatase (units/L)
f
Total protein levels
NOD
B6g7
Protein per 100,000 islet cells (μg)
g
Granule presentation between NOD and B6g7
IL-2 (units/ml)
IIT-3
9B9
h
Diabetes incidence in our NOD colony
Monitoring female (n=61)
Untreated female (n=12)
Monitoring male (n=48)
ns
Diabetes incidence (%)
Weeks of age
i
Insulitis development in mice from the monitoring cages
6-week female
16-week female
Insulitis score
****
6-week
16-week
Insulitis score
0. No infiltration
1. Peri-insulitis
2. Intra-insulitis (< 25%)
3. Intra-insulitis (25-50%)
4. Intra-insulitis (> 50%)

Supplementary Fig. 1. Validation of granule isolation and diabetes development.

a. Responses of two $CD4^+$ T cell hybridomas during in vitro stimulation with intact insulin and three peptides associated with insulin B-chain, including B:9-23 (SHLVEALYLVCGERG) that contains both G20 (VEALYLVCG, underscored with blue line) and E21 (EALYLVCGE, underscored with red line) binding registers, Syn-G20 (TEGVEALYLVCGGGS) containing G20 with surrogate flanks, and Syn-E21 (TEGEALYLVCGEGGS) containing E21 with surrogate flanks.

b. Peptide concentration required for each hybridoma to reach half maximal responses (EC50) from three independent measurements. The results indicate comparable sensitivity of the two hybridomas. ns, not significant; Two-tailed paired t test.

c. Schematics of isolating subcellular fractions from islets of 4-week-old female NOD mice, created in BioRender. Wan, X. (2022) BioRender.com/g66g962

d. Response of 9B9 and IIT-3 T cells to indicated subcellular fractions offered to the C3.g7 APC. Data (mean ± s.e.m) summarize results from n=3 in three independent experiments; each symbol represents an experiment.

e. ELISA analysis of acid phosphatase levels in indicated fractions. Data (mean ± s.e.m) summarize results from n=3 in three independent experiments; each symbol represents an experiment.

f. Bicinchoninic acid (BCA) protein assay of the contents from indicated subcellular fractions isolated from 4-week-old female NOD and B6g7 mice. Data (mean ± s.e.m) summarize results from n=2 in two independent experiments. ns, not significant; Two-way ANOVA test.

g. Response of IIT-3 and 9B9 T cells to indicated subcellular fractions isolated from 4-week-old female NOD and B6g7 mice. Data (mean ± s.e.m) summarize results from n=2 in two independent experiments. ns, not significant; Two-way ANOVA test.

h. Diabetes incidence in female NOD mice (n shown in figure) in separate monitoring cages versus untreated control mice that were monitored alongside mice given PBS or chloroquine. Diabetes incidence of male NOD mice in the monitoring cages is also shown. ns, not significant; Log-rank (Mantel-Cox) test.

i. Insulitis development between 6-week (n=60 islets) and 16-week (n=60 islets) non-diabetic female NOD mice in the monitoring cages. Shown are representative H&E images and quantification of insulitis scores of 60 islets from five mice per age. ****$P < 0.0001$; Mann-Whitney test, two-tailed.

a

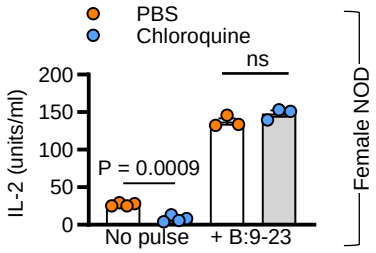

b

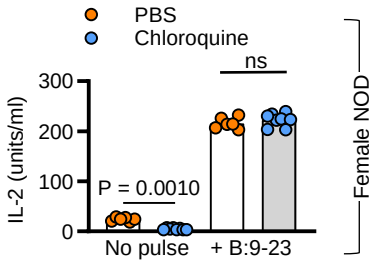

c

HIP sequences (left-right)	Source protein	PBS	Chloroquine
EVED-TPVRSGTNPQM	InsC-IAPP	X	
EVED-TPVRSGTNPQm*	InsC-IAPP	X	X
EVED-TPVRSGTNP	InsC-IAPP	X	
EVED-NAARDPNRESLDFL	InsC-IAPP	X	
EVED-NAARDPNRESLDF	InsC-IAPP	X	
EVED-EVEDPQVEQ	InsC-Ins1C	X	
EVED-EVEDPQ	InsC-InsC	X	
LAL-NAARDPNRESLDF	InsC-IAPP	X	
LAL-EVEDPQVAQ	InsC-InsC	X	
LAL-EVEDPQ	InsC-InsC	X	

* Oxidation (M)

d

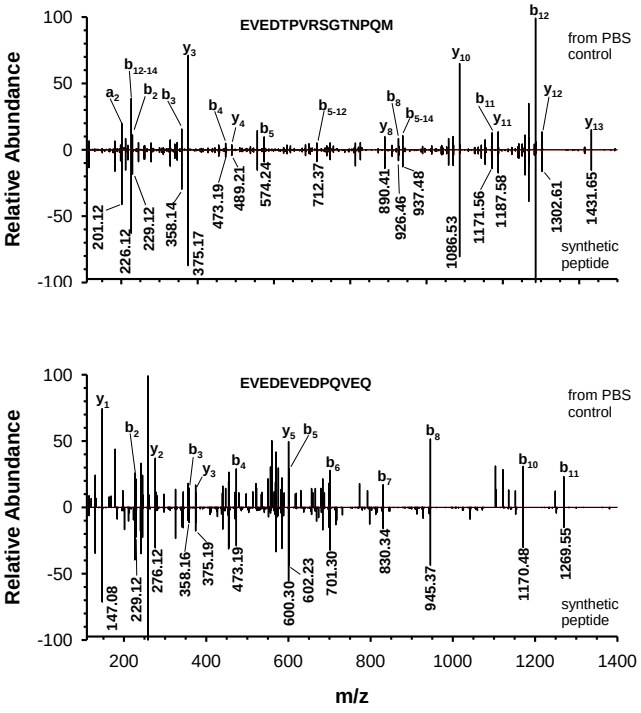

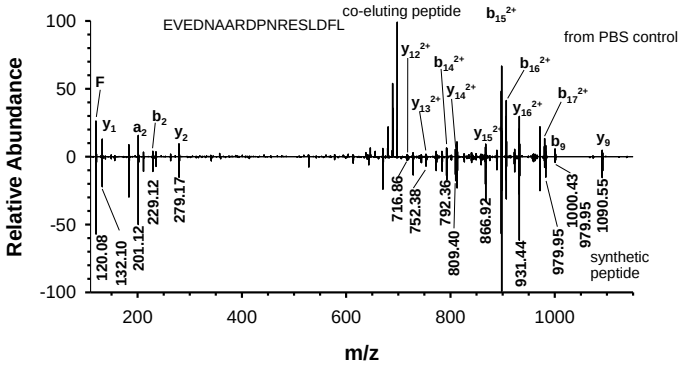

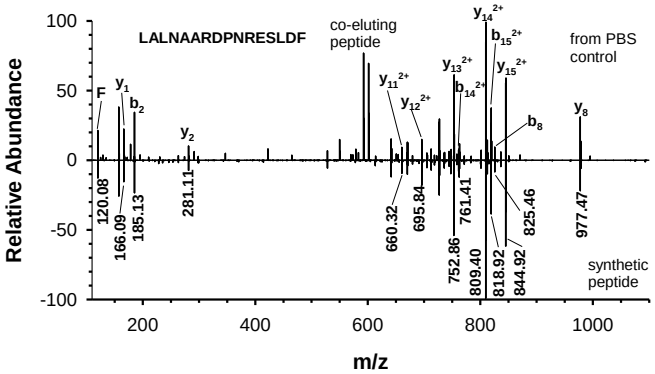

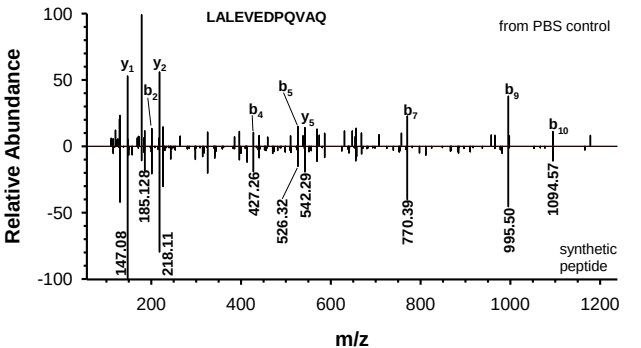

Supplementary Fig. 2. Treatment with chloroquine diminishes the production of hybrid insulin peptides in crinosomes.

a. Presentation of G20 by dispersed islet cells (islet resident macrophages) from 4-week-old female NOD mice given PBS or chloroquine without antigen pulse (n=20 for each condition in two independent experiments) or during pulse with the B:9-23 peptide (10 µM) (n=9 for each condition in two independent experiments). Data (mean ± s.e.m) summarize results from two independent experiments; each symbol represents one biological replicate including 2-5 mice. ns, not significant; ***P = 0.0009; Mann-Whitney test, two-tailed.

b. Spontaneous presentation of G20 by blood leukocytes isolated from 4-week-old female NOD mice given PBS (n=6) or chloroquine (n=8) without antigen pulse or during pulse with the B:9-23 peptide (10 µM). Data (mean ± s.e.m) summarize results from two independent experiments; each symbol represents results from an individual mouse. ns, not significant; ***P =0.0010; Mann-Whitney test, two-tailed.

c. Summary of hybrid insulin peptides (HIPs) identified in crinosomes isolated from PBS control and chloroquine-treated mice. The left and right parts of the HIP sequences are separated by a hyphen. Also noted are the source protein regions of the left and right parts of the HIPs. InsC; proinsulin C-peptide segments that are homologous between proinsulin-1 and proinsulin-2. Ins1C; proinsulin-1 C-peptide. IAPP; islet amyloid polypeptide.

d. Mirror plots illustrating a complete match between biological (top) and synthetic standard (bottom) for HIPs identified in crinosomes isolated from PBS-treated mice.

a

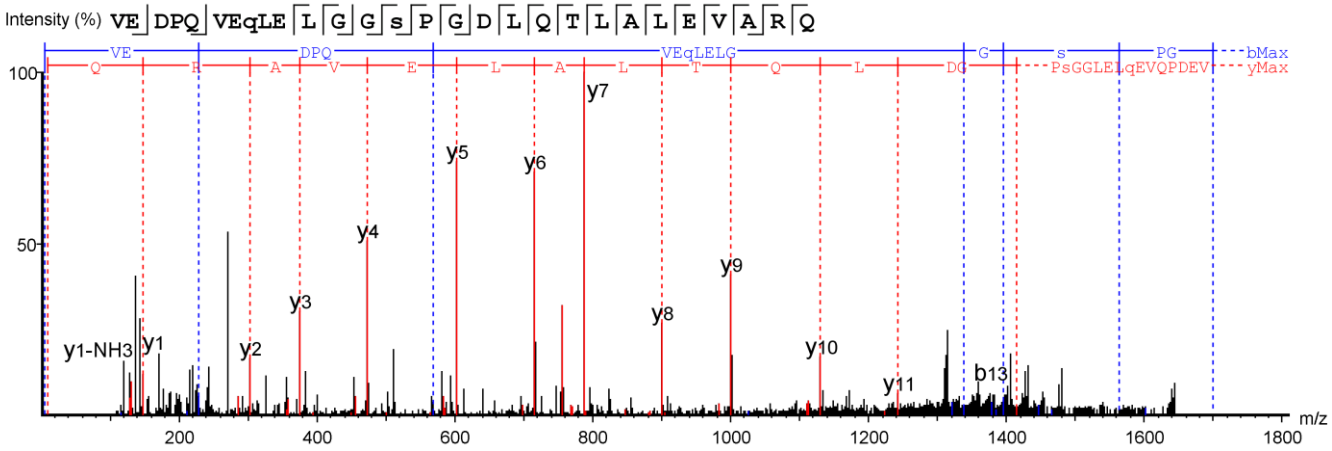
Intensity (%)
VE DPQ VEqLE L G G s P G D L Q T L A L E V A R Q
bMax
yMax
y1-NH3
y1
y2
y3
y4
y5
y6
y7
y8
y9
y10
y11
b13
m/z

b

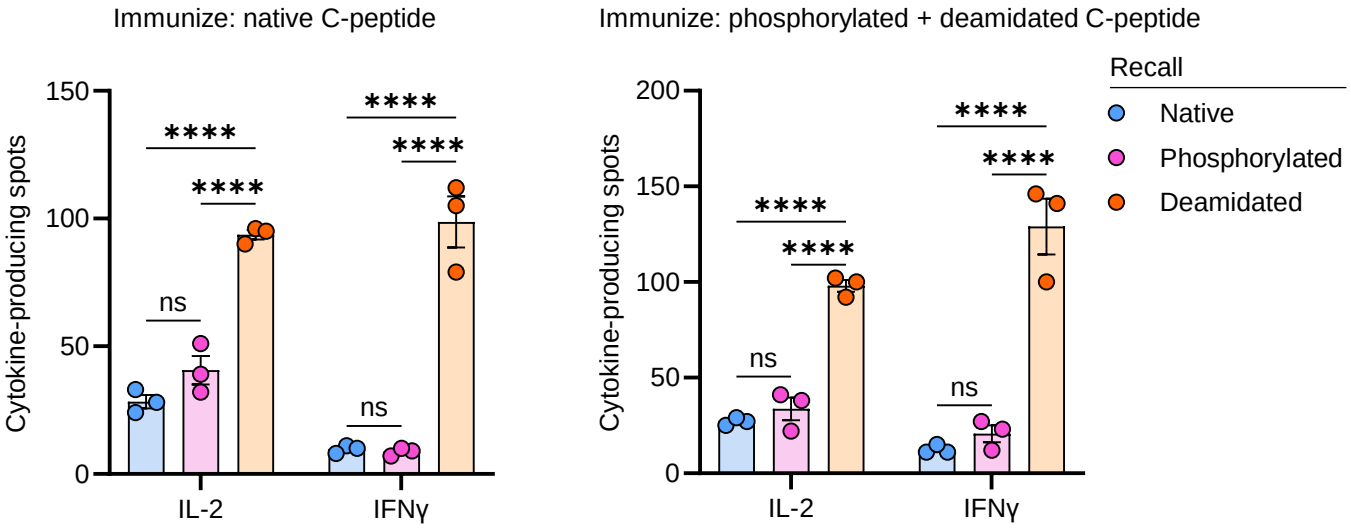
Immunize: native C-peptide
Immunize: phosphorylated + deamidated C-peptide
Cytokine-producing spots
IL-2
IFNγ
ns
****
Recall
Native
Phosphorylated
Deamidated

Supplementary Fig. 3. Analysis of T-cell responses to native and phosphorylated C-peptides.

a. An MS spectrum showing an example of an insulin-1 C-peptide sequence identified in the crinosome peptidome from mice given PBS control. The lowercase letters denote the positions of the deamidated glutamine (q) and phosphorylated serine (s) residues.

b. ELISPOT assay assessing T cell responses during recall with the full-length native insulin-1 C-peptide (EVEDPQVEQLELGGSPGDLQTLAEVARQ), the phosphorylated C-peptide (EVEDPQVEQLELGGsPGDLQTLAEVARQ), or the deamidated C-peptide (GDLQTLAEVARq(E)) in mice immunized with either the native C-peptide (left) or a mixture of the phosphorylated and deamidated C-peptides (right). Data (mean ± s.e.m) summarize results from individual mice (n=3). ns, not significant; Two-way ANOVA analysis with Tukey's multiple comparisons test.

a

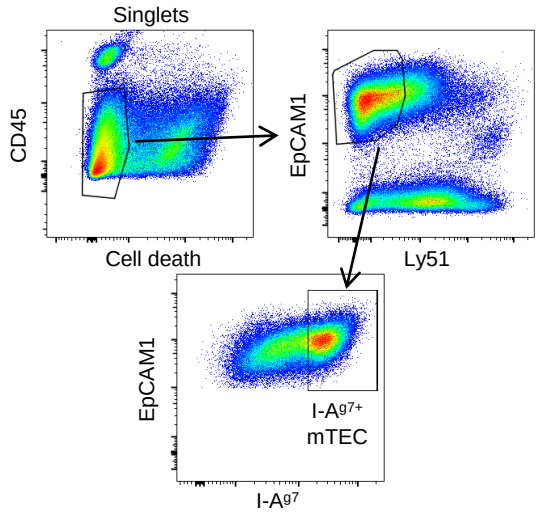

b

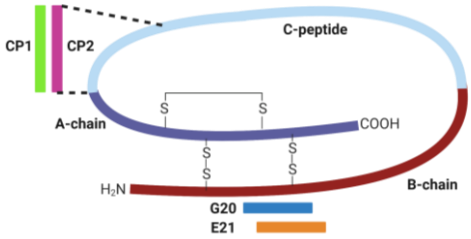

Peptides	Sequences	Gene
CP1	GDLQTLALEVARQ	*Ins1*
CP2	GDLQTLALEVAQQ	*Ins2*
G20	VEALYLVCG	*Ins1/Ins2*
E21	EALYLVCGE	*Ins1/Ins2*

c

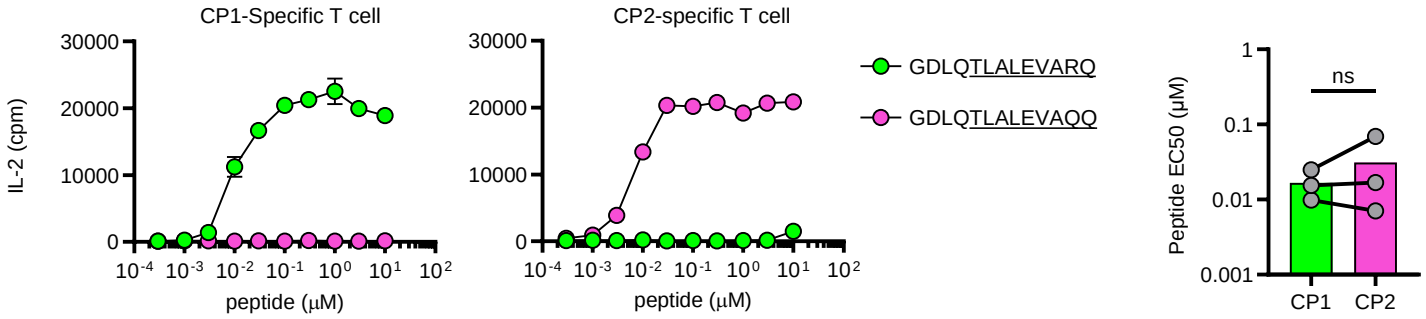

d

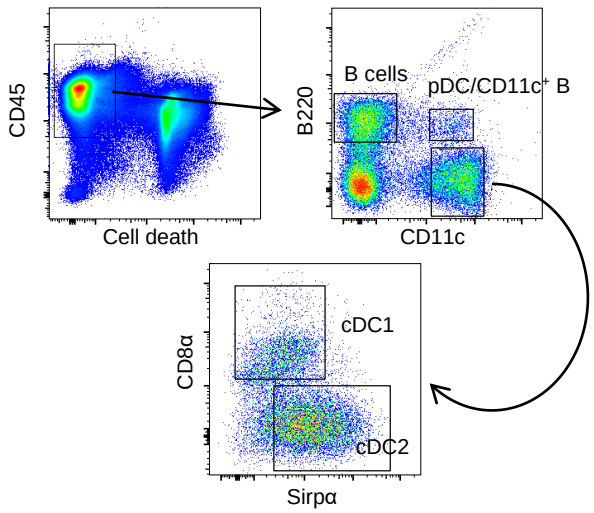

e

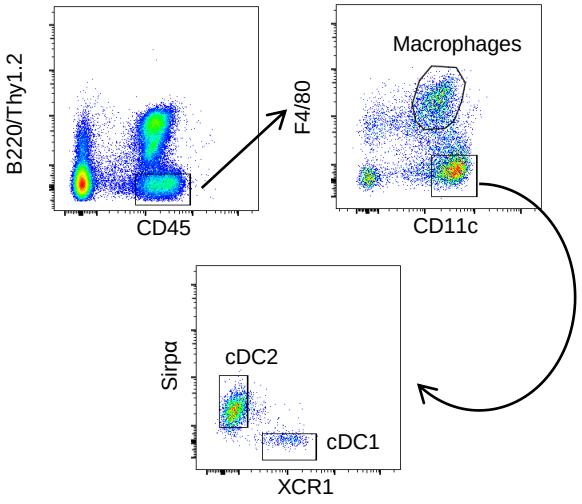

Supplementary Fig. 4. Analysis of insulin epitope presentation in the thymus.

a. Sorting strategy for isolating MHC-II (I-A^{g7})$^+$ mTECs from thymi of 3-6-week-old NOD mice. CD45$^-$ cells were enriched from the thymic cells by magnetic beads and were stained with indicated markers for FACS-sorting. I-A^{g7+} mTECs were sorted as CD45$^-$ Epcam1$^+$Ly51^{low}I-A^{g7+}. Preliminary experiments showed that about 95% of cells in the CD45$^-$Epcam1$^+$Ly51^{low}I-A^{g7+} population also express UEA-1, a mature mTEC marker.

b. Illustration of four epitopes known to bind to I-A^{g7} from insulin B-chain and C-peptide. The four epitopes were tested for their spontaneous presentation in the thymus.

c. Responses of two CD4$^+$ T cell hybridomas during in vitro stimulation with epitopes from insulin-1 (CP1; GDLQTLALEVARQ) and insulin-2 (CP2; GDLQTLALEVAQQ) C-peptide using the C3.g7 APC. The 9-mer binding core is underlined. The data show that the two hybridomas are specific to their respective epitopes and are non-cross-reactive.

d. Sorting strategy for isolating B cells (CD45$^+$B220$^+$CD11c$^-$), pDCs/CD11c+ B cells (CD45$^+$B220$^+$CD11c$^+$), cDC1 (CD45$^+$B220$^-$CD11c$^+$XCR1$^+$), and cDC2 (CD45$^+$B220$^-$ CD11c$^+$Sirpα$^+$) from thymus of 3-6-week-old NOD mice.

e. Sorting strategy for isolating the resident macrophages (CD45$^+$B220$^-$Thy1.2$^-$ CD11c$^+$F4/80$^+$), cDC1(CD45$^+$B220$^-$Thy1.2$^-$CD11c$^+$F4/80$^-$XCR1$^+$Sirpα$^-$), and cDC2 (CD45$^+$B220$^-$Thy1.2$^-$CD11c$^+$F4/80$^-$XCR1$^-$Sirpα$^+$) from islets of 8-10-week-old female NOD mice.

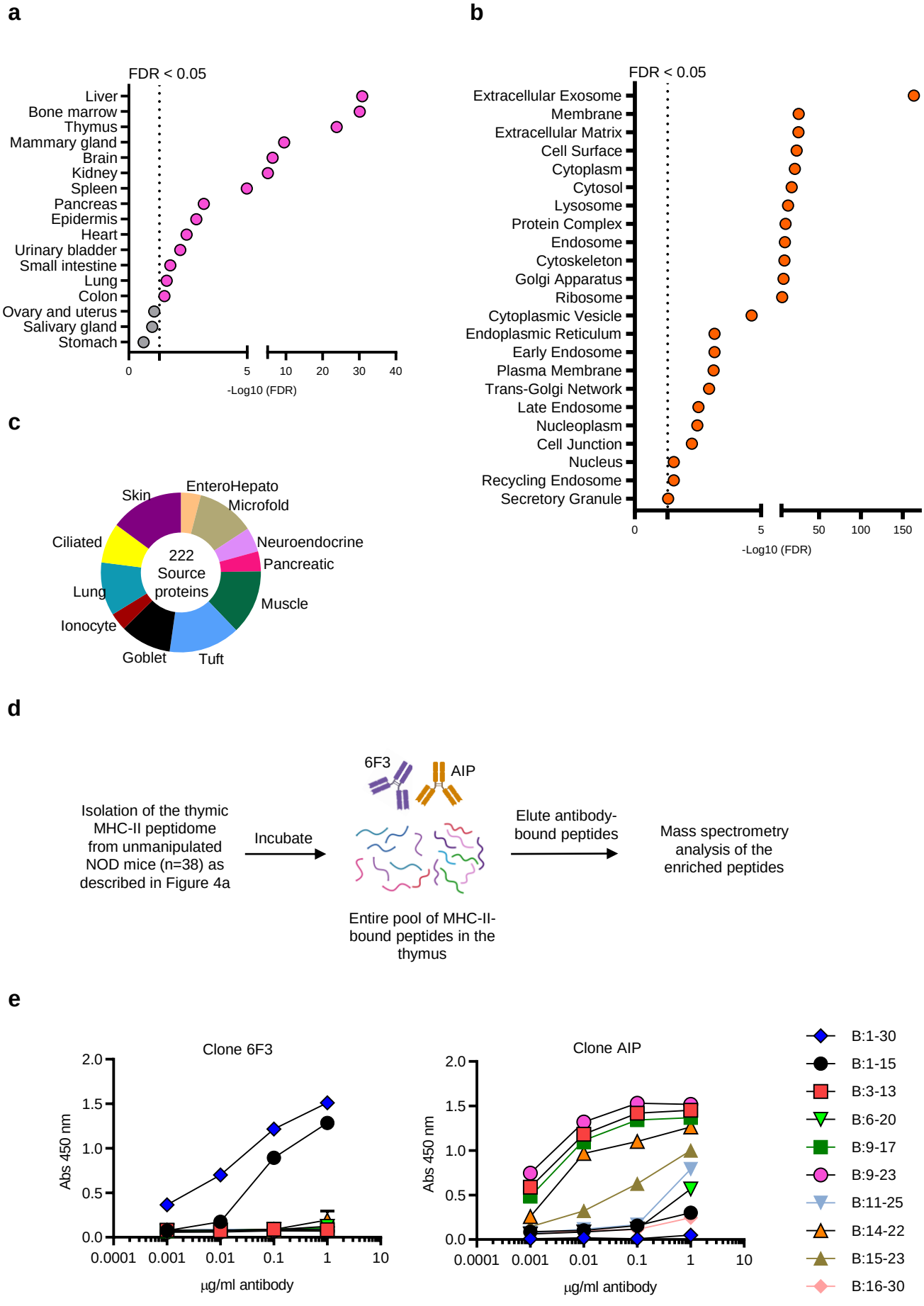
a
FDR < 0.05
Liver
Bone marrow
Thymus
Mammary gland
Brain
Kidney
Spleen
Pancreas
Epidermis
Heart
Urinary bladder
Small intestine
Lung
Colon
Ovary and uterus
Salivary gland
Stomach
0
5
10
20
30
40
-Log10 (FDR)
b
FDR < 0.05
Extracellular Exosome
Membrane
Extracellular Matrix
Cell Surface
Cytoplasm
Cytosol
Lysosome
Protein Complex
Endosome
Cytoskeleton
Golgi Apparatus
Ribosome
Cytoplasmic Vesicle
Endoplasmic Reticulum
Early Endosome
Plasma Membrane
Trans-Golgi Network
Late Endosome
Nucleoplasm
Cell Junction
Nucleus
Recycling Endosome
Secretory Granule
0
5
50
100
150
-Log10 (FDR)
c
Skin
EnteroHepato
Microfold
Ciliated
Neuroendocrine
Pancreatic
222
Source
proteins
Lung
Muscle
Ionocyte
Goblet
Tuft
d
Isolation of the thymic MHC-II peptidome from unmanipulated NOD mice (n=38) as described in Figure 4a
Incubate
6F3
AIP
Entire pool of MHC-II-bound peptides in the thymus
Elute antibody-bound peptides
Mass spectrometry analysis of the enriched peptides
e
Clone 6F3
Clone AIP
Abs 450 nm
2.0
1.5
1.0
0.5
0.0
0.0001
0.001
0.01
0.1
1
10
µg/ml antibody
B:1-30
B:1-15
B:3-13
B:6-20
B:9-17
B:9-23
B:11-25
B:14-22
B:15-23
B:16-30

Supplementary Fig. 5. Analysis of the thymic MHC-II peptidome.

a. Tissue localization analysis of the source proteins of the identified peptides in the thymic MHC-II peptidome. The source proteins were mapped 14 different peripheral tissues that meet the cut-off (FDR < 0.05) defined by the DAVID tool. Three tissues were below the cut-off and were excluded from downstream analysis.

b. Cellular component analysis of the source proteins of the identified peptides in the thymic MHC-II peptidome. The results depict that the source proteins belong to various cellular components and locations that meet the FDR cut-off).

c. Overlay of the thymic peptidome data with single-cell RNA sequencing analysis of post-Aire mimetic mTEC subtypes with PTA expression reflecting different peripheral cell types.

d. Schematic of the workflow for enriching insulin B-chain-derived peptides from the thymic MHC-II peptidome by antibody capture, created in BioRender. Wan, X. (2024) BioRender.com/s20b261. The MHC-II-bound peptides were isolated from unmanipulated NOD mice (3-6-week-old; n=38) and were incubated with a mixture of two monoclonal antibodies (6F3 and AIP) recognizing different segments of the insulin B-chain. The antibody-bound peptides were eluted and analyzed by mass spectrometry.

e. The antibody 6F3 and AIP recognize complementary peptide segments spanning the full-length of the insulin B-chain (B:1-30). Data depict ELISA analysis of the reactivity of the 6F3 and AIP antibodies to indicated plate-bound B-chain synthetic peptides.

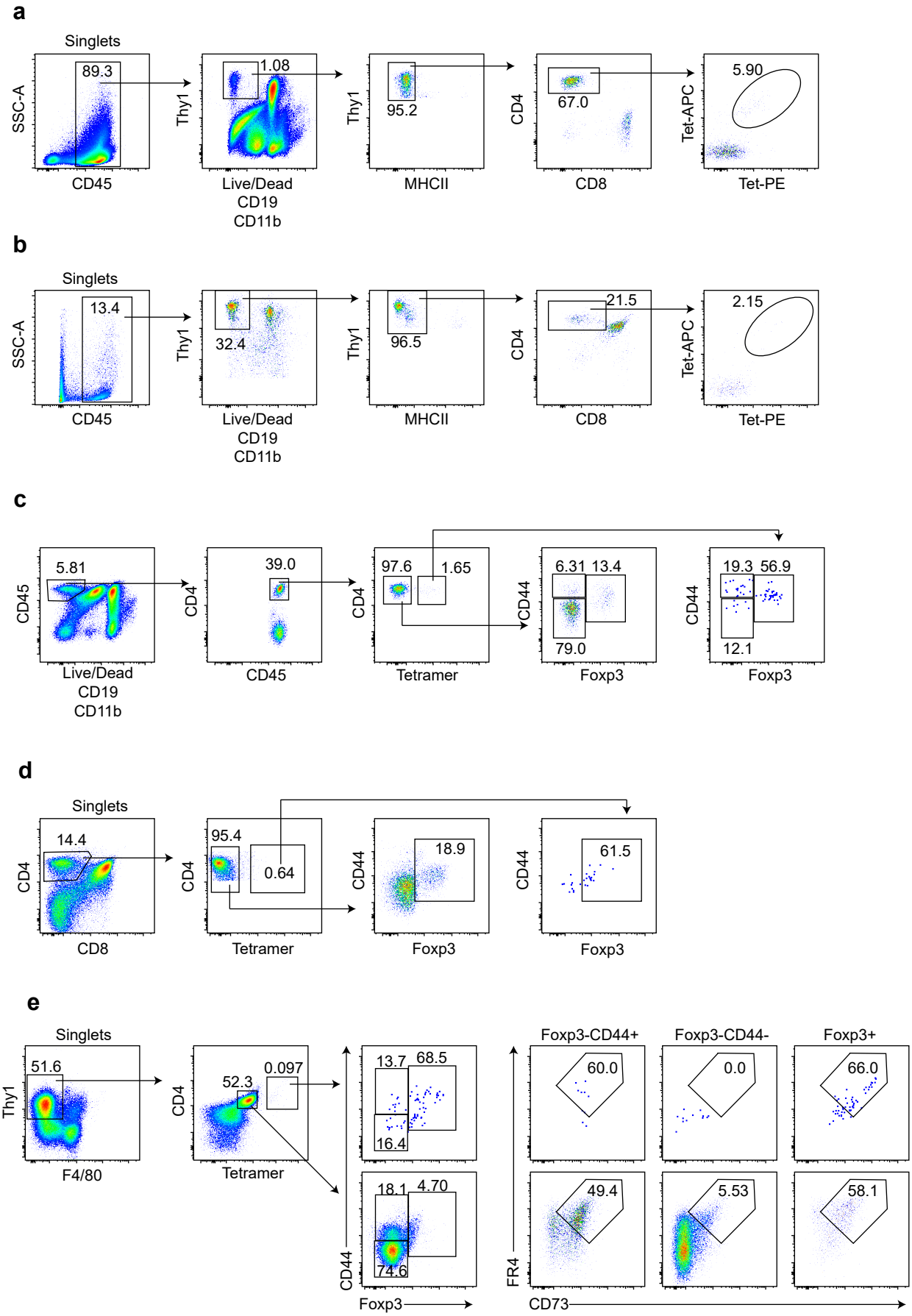
a
Singlets
89.3
SSC-A
CD45
Thy1
1.08
Live/Dead
CD19
CD11b
Thy1
95.2
MHCII
CD4
67.0
CD8
Tet-APC
5.90
Tet-PE
b
Singlets
13.4
SSC-A
CD45
Thy1
32.4
Live/Dead
CD19
CD11b
Thy1
96.5
MHCII
CD4
21.5
CD8
Tet-APC
2.15
Tet-PE
c
CD45
5.81
Live/Dead
CD19
CD11b
CD4
39.0
CD45
CD4
97.6
1.65
Tetramer
CD44
6.31
13.4
79.0
Foxp3
CD44
19.3
56.9
12.1
Foxp3
d
Singlets
CD4
14.4
CD8
CD4
95.4
0.64
Tetramer
CD44
18.9
Foxp3
CD44
61.5
Foxp3
e
Singlets
Thy1
51.6
F4/80
CD4
52.3
0.097
Tetramer
13.7
68.5
16.4
18.1
4.70
74.6
CD44
Foxp3
Foxp3-CD44+
Foxp3-CD44-
Foxp3+
60.0
0.0
66.0
49.4
5.53
58.1
FR4
CD73

Supplementary Fig. 6. Analysis of insulin epitope presentation in the thymus.

a. Gating strategy for detecting tetramer positive antigen specific T cells in Secondary lymphoid tissues (SLOs). E21 specific T cells were used as an example. SLOs from 6-8-week-old female NOD mice were meshed through strainer to prepare single cells. After red blood cells lysis, cells were stained with PE or APC-streptavidin conjugated tetramers for 1h at RT and then stained with other surface markers as indicated.

b. Gating strategy for detecting tetramer positive antigen specific T cells in thymus. E21 specific thymocytes were used as an example. Thymic tissues from 6-8-week-old female NOD mice were meshed through strainer to prepare single cells. Cells were stained with PE or APC-streptavidin conjugated tetramers for 1h at RT and then stained with other surface markers as indicated.

c. Gating strategy for detecting Treg development for tetramer positive antigen specific T cells in SLOs. E21 specific T cells were used as an example. SLOs from 6-8-week-old female NOD mice were meshed through strainer to prepare single cells. After red blood cells lysis, cells were stained with APC-streptavidin conjugated tetramers for 1h at RT and then stained with other surface markers as indicated. Then cells were fixed and permeabilized staining Foxp3.

d. Gating strategy for detecting Treg development for tetramer positive antigen specific T cells in thymus. E21 specific T cells were used as an example. . Thymic tissues from 6-8-week-old female NOD mice were meshed through strainer to prepare single cells. Cells were stained with APC-streptavidin conjugated tetramers for 1h at RT and then stained with other surface markers as indicated. Then cells were fixed and permeabilized staining Foxp3.

e. Gating strategy for detecting Treg and anergic T cell development for tetramer positive antigen specific T cells in SLOs. E21 specific T cells were used as an example. SLOs from 6-8-week-old female NOD mice were meshed through strainer to prepare single cells. After red blood cells lysis, cells were stained with APC-streptavidin conjugated tetramers for 1h at RT and then stained with other surface markers as indicated. Then cells were fixed and permeabilized staining Foxp3.

a

Thymic epitope set			Islet epitope set		
Epitope	**Description**	**Sequence**	**Epitope**	**Description**	**Sequence**
CP2	Proinsulin-2 C-peptide 53-63	GDLQTLALEVAQQ	**CP1d**	Deamidated proinsulin-1 C-peptide 51-61 (Q61E)	GDLQTLALEVARE
E21	Proinsulin B-chain 13-21	EALYLVCGE	**G20**	Proinsulin B-chain 12-20	VEALYLVCG
DBP	Vitamin D binding protein 387-405	TQSPLLKRQLTSFIEKGQE	**2.5HIP**	C-peptide-ChgA hybrid insulin peptide	LQTLAL-WSRMD
ZnT8	Zinc transporter 8 313-326	ILSVHVATAASQDS	**6.9HIP**	C-peptide-IAPP hybrid insulin peptide	LQTLAL-NAARD

b

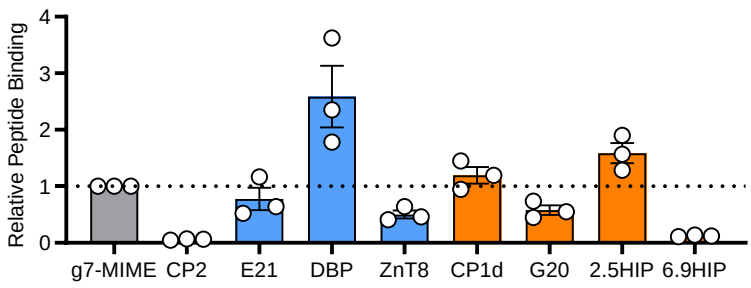

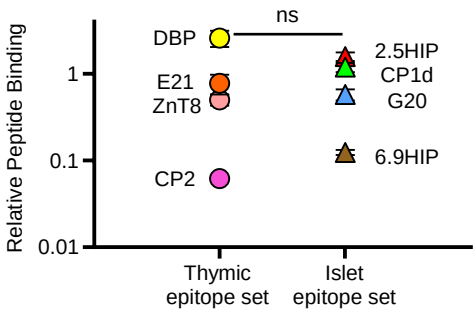

c

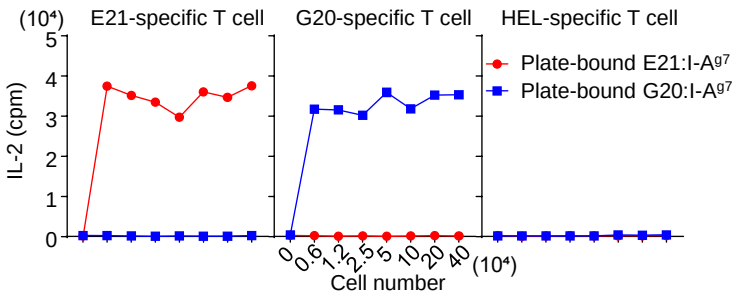

d

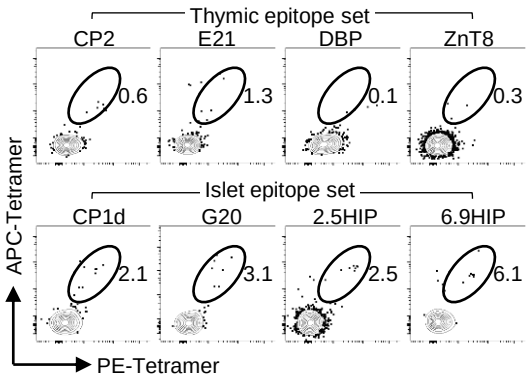

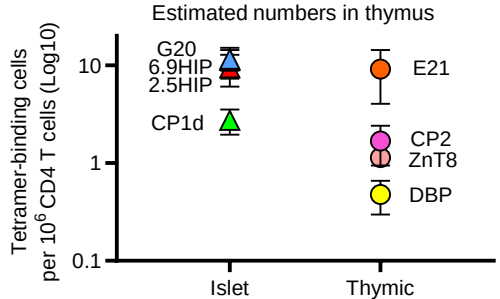

e

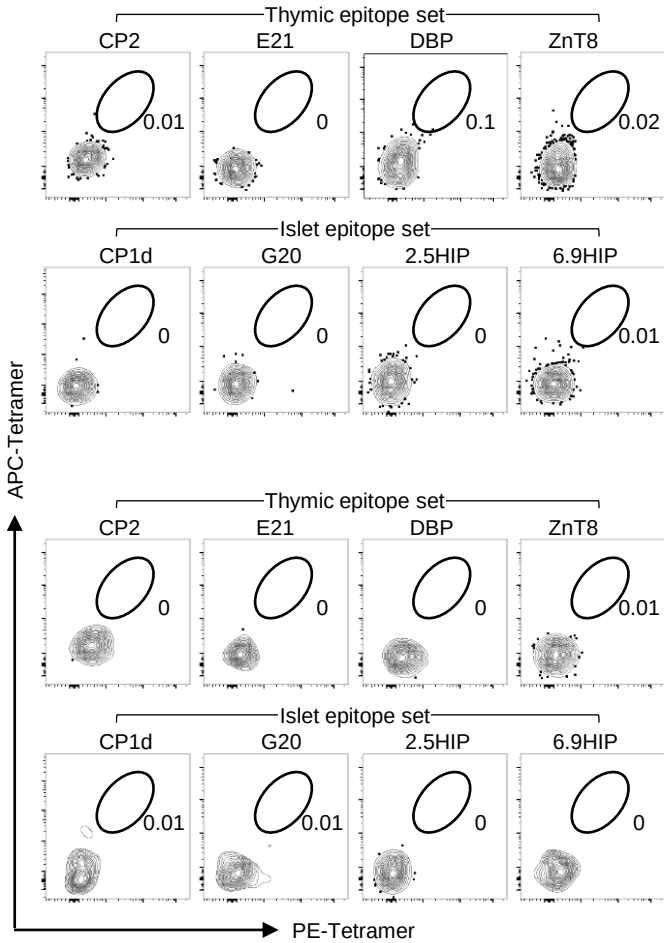

Supplementary Fig. 7. Analysis of tetramer-binding CD4$^+$ T cells reactive to epitopes presented in the thymus versus pancreatic islets.

a. A table depicting epitopes that were used for tetramer production and T cell analyses. A total of eight epitopes were grouped in two sets. The “thymic epitope set” comprises four epitopes that were detected by the thymic antigen presentation and immunopeptidome analysis. The “islet epitope set” contains four epitopes that were known to be recognized by diabetogenic CD4$^+$ T cells and were below the detection threshold of the thymic peptidome analysis. The sequences listed for each epitope were identical to those used for producing tetramers.

b. Peptide binding assay depicting relative I-A^{g7}-binding affinities of indicated peptides. The data show relative binding affinities normalized to a reference peptide (g7-MIME) in three independent experiments. The dot plot (right) shows comparable overall binding affinity of epitopes grouped into the thymic or islet epitope set. ns, not significant; Mann-Whitney test, two-tailed.

c. Responses of the E21- and G20-specific CD4$^+$ T cell hybridomas to plate-coated E21:I-A^{g7} and G20-20:I-A^{g7} monomers. An HEL-specific T cell hybridoma was included as a negative control.

d. Tetramer-binding CD4$^+$ single-positive T cells for indicated epitopes in thymus of 6-8-week-old female NOD mice. The FACS plots depict double-positive tetramer-binding populations (gated on CD45$^+$B220$^-$CD8$^-$CD11b$^-$I-A^{g7-}Thy1.2$^+$CD4$^+$) in cells with magnetic enrichment. The dot plot shows the numbers of tetramer-binding T cells for each epitope (mean $\pm$ s.e.m) quantified from 4-8 individual mice in four independent experiments.

e. Tetramer binding of CD8 T cells in SLOs and thymus. The data show minimal tetramer binding when gated on CD8 T cells.

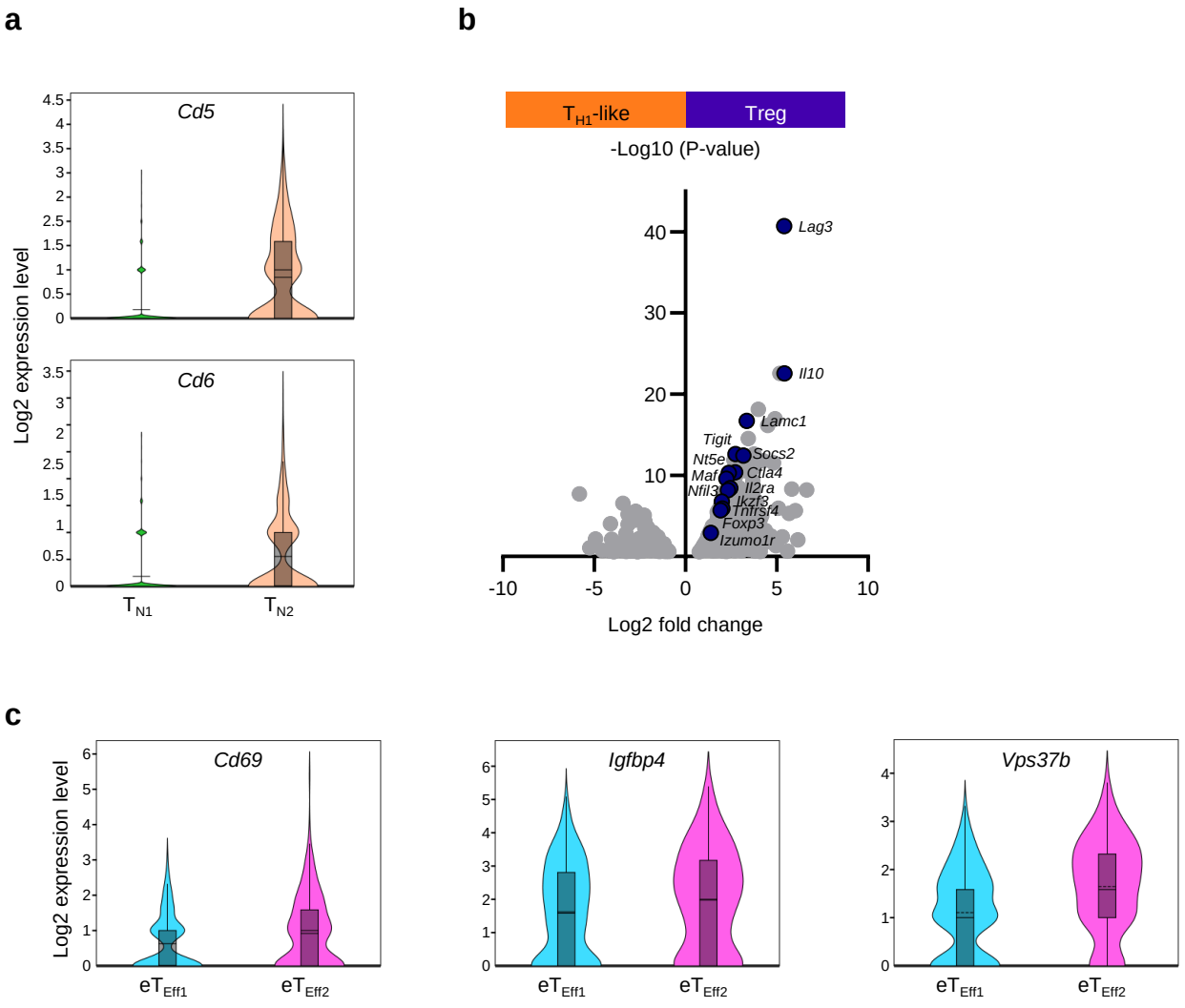
a
b
c
Cd5
Cd6
Log2 expression level
T_{N1}
T_{N2}
T_{H1}-like
Treg
-Log10 (P-value)
Log2 fold change
Lag3
Il10
Lamc1
Tigit
Nt5e
Socs2
Mafk
Ctla4
Nfil3
Il2ra
Ikzf3
Tnfrsf4
Foxp3
Izumo1r
Cd69
Igfbp4
Vps37b
eT_{Eff1}
eT_{Eff2}

Supplementary Fig. 8. Single-cell RNA sequencing analysis of tetramer-binding CD4$^+$ T cells in the thymic and islet epitope set.

a. Differential expression of *Cd5* and *Cd6* transcript between the two naïve T cell clusters.

b. Signature genes representing the Treg cell cluster relative to the T_{H1}-like cluster.

c. Differential expression of *Cd69, Igfbp4,* and *Vps37b* transcripts between the two early effector clusters.

• All the genes described in this Figure meet the statistical cut-off (adjusted $P < 0.05$) using the Benjamini-Hochberg correction for multiple tests.

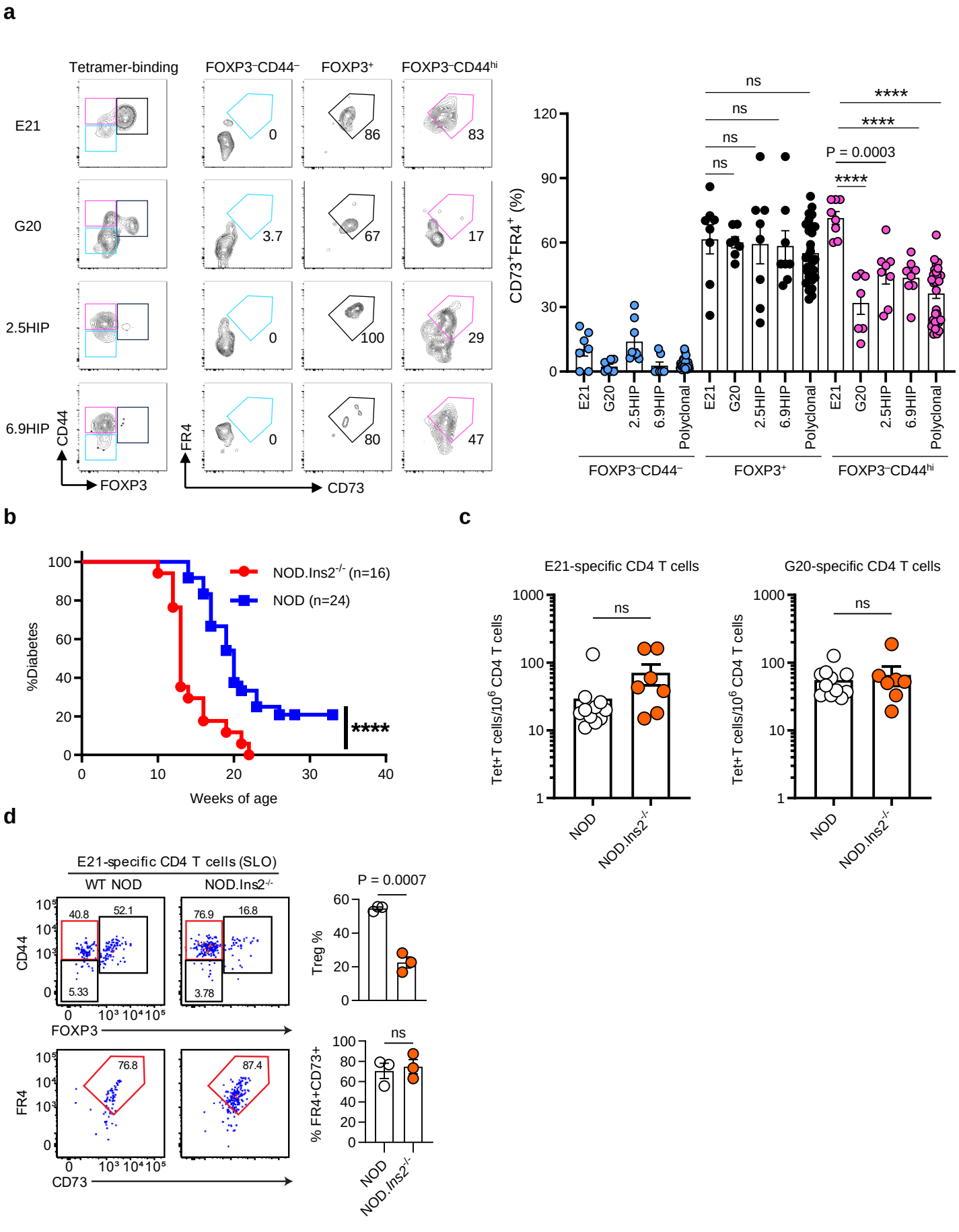
a
Tetramer-binding
FOXP3⁻CD44⁻
FOXP3⁺
FOXP3⁻CD44ʰⁱ
E21
G20
2.5HIP
6.9HIP
0
86
83
3.7
67
17
0
100
29
0
80
47
CD44
FOXP3
FR4
CD73
CD73⁺FR4⁺ (%)
ns
****
P = 0.0003
E21
G20
2.5HIP
6.9HIP
Polyclonal
FOXP3⁻CD44⁻
FOXP3⁺
FOXP3⁻CD44ʰⁱ
b
%Diabetes
Weeks of age
NOD.Ins2-/- (n=16)
NOD (n=24)
****
c
E21-specific CD4 T cells
G20-specific CD4 T cells
Tet+T cells/10⁶ CD4 T cells
ns
NOD
NOD.Ins2-/-
d
E21-specific CD4 T cells (SLO)
WT NOD
NOD.Ins2-/-
40.8
52.1
5.33
76.9
16.8
3.78
76.8
87.4
CD44
FOXP3
FR4
CD73
P = 0.0007
Treg %
% FR4+CD73+
ns
NOD
NOD.Ins2-/-

Supplementary Fig. 9. Analysis of anergy-associated phenotypes in tetramer-binding CD4$^+$ T cells.

a. Flow cytometry analysis of two anergy markers FR4 and CD73 in tetramer-binding CD4$^+$ T cells for indicated epitopes. The analysis was based on three subsets classified by the expression FOXP3 and CD44. The percentage of CD73$^+$FR4$^+$ double-positive anergic T cells among each of the three subsets are summarized. (n=8: E21, n=7: G20, n=8: HIP2.5, n=7: 6.9HIP, n=31: polyclonal T cells). ns, not significant; ***P = 0.0003; ****P < 0.0001; One-way ANOVA with Sidak's multiple comparisons test.

b. Incidence of diabetes development in female WT NOD and NOD.Ins2$^{-/-}$ mice. ****P < 0.0001; Log-rank test.

c. The numbers of E21- and G20-reactive tetramer-binding CD4$^+$ T cells estimated in SLOs of age/sex-matched NOD (n=11) and NOD.*Ins2*$^{-/-}$ mice (n=7). Each symbol represents results from an individual mouse. ns, not significant; Mann-Whitney test, two-tailed.

d. Flow cytometry analysis of FR4 and CD73 expression in the FOXP3$^-$CD44^{hi} subset of E21 tetramer-binding CD4$^+$ T cells between WT NOD and NOD.*Ins2*$^{-/-}$ mice (lower). The gating of the FOXP3$^-$CD44^{hi} subset was depicted in FACS plots showing the CD44 and FOXP3 expression in E21 tetramer-binding T cells (upper). The bar graph (upper) shows the significant decrease in the FOXP3$^+$ Treg population in the NOD.*Ins2*$^{-/-}$ mice, whereas the frequencies (lower) of CD73$^+$FR4$^+$ double-positive anergic T cells in the FOXP3$^-$CD44^{hi} subset were comparable between the two strains. Data (mean ± s.e.m) are from n=3 in three independent experiments. ns, not significant; ***P = 0.0007; unpaired t-test, two-tailed.